First-principles calculations of the local magnetic properties of face-centred cubic disordered Fe-Pd alloys

1993 J. Phys.: Condens. Matter 5 5343

(http://iopscience.iop.org/0953-8984/5/30/014)

J. Phys.: Condens. Matter 5 (1993) 5343–5352. Printed in the UK

First-principles calculations on the local magnetic properties of face-centred cubic disordered Fe–Pd alloys

Cai Jian-Wang†, Luo He-Lie†, Zeng Zhi‡ and Zheng Qing-Qi‡

† State Key Laboratory of Magnetism, Institute of Physics, Academia Sinica, Beijing 100080, People's Republic of China

‡ Institute of Solid State Physics, Academia Sinica, Hefei 230031, People's Republic of China

Received 8 March 1993

Abstract. Self-consistent-field electronic structure calculations were performed for embedded clusters representing FCC disordered Fe–Pd alloys. The discrete variational method was employed in the framework of local-spin-density theory. The hyperfine magnetic fields and the magnetic moments on several distinct Fe sites and Pd sites in the Fe–Pd alloys were derived from the calculations. The results for magnetic moments show that the Fe–Pd alloys are strong ferromagnets and that the Fe magnetic moment is almost independent of the number of Pd nearest neighbours, slightly increasing with increasing number of Pd nearest neighbours, while Pd atoms are strongly polarized. When a Pd atom is surrounded by six Fe and six Pd nearest neighbours, it has a maximum induced magnetic moment. The changes in hyperfine fields due to the variation in the number of Pd nearest neighbours are in good agreement with experiment.

1. Introduction

For nearly a century, great efforts have been made to investigate alloys which show an abnormal temperature dependence of their physical properties below the magnetic ordering temperature, i.e. the coefficient of thermal expansion, the elastic constant and the mean magnetic moment [1,2]. These alloys are called Invar alloys. Fe–Pd alloys exhibit the so-called 'Invar behaviour', a large magnetovolume effect in the Fe-rich region with an FCC crystalline structure [3,4]. In addition, the paramagnetism of pure Pd is drastically affected by the addition of the 3d transition metals; the alloys with Cr and Mn exhibit anitferromagnetic tendencies [5], while those with Fe and Co become ferromagnetic even at very low 3d concentrations [6,7]. Thus Fe–Pd alloys have been of special interest.

The magnetic properties of Fe–Pd alloys have been extensively studied by Cable *et al* [8], who investigated the distribution of magnetic moments in FCC Fe–Pd alloys by means of neutron-scattering and magnetization measurements. They found that, in these alloys, Fe has a moment of about $3.0\mu_B$, a moment that is almost independent of concentration, while the average Pd moment varies with concentration and approaches a maximum of about $0.4\mu_B$ per atom in the concentrated alloys. Mössbauer spectroscopy is an effective technique for studying the local properties of condensed matter, which allows measurement of the hyperfine interactions between the probe nucleus and its electronic environment. Zhang *et al* [9] analysed a series of Mössbauer spectra of Fe–Pd alloys, and they came to the conclusion that the average hyperfine magnetic fields of these FCC alloys gradually decrease with increasing Pd concentration.

Many aspects of knowledge about the Fe–Pd alloys have been obtained from experimental investigations; however, there seems to be hardly any theoretical study on

0953-8984/93/305343+10$07.50

their local magnetic properties using first-principles theory. In spite of the considerable theoretical work on the giant moment phenomenon of Fe impurities in the dilute Fe–Pd alloys [10–14], understanding of the concentrated Fe–Pd alloys is far from complete and many questions have been left unanswered. In the present work, we shall investigate the influence of the local environment on the electronic structures, magnetic moments and hyperfine fields in the FCC disordered Fe–Pd alloys by means of first-principles molecular cluster calculations within the framework of the discrete variational method (DVM), which has been shown to be highly successful in describing the properties of transition metals and intermetallic compounds [15–17]. We focus our attention on the electronic and magnetic properties of the central Fe sites and the central Pd sites in several clusters and give a theoretical description of the local magnetic properties of FCC disordered Fe–Pd alloys.

In the following section, we present the theoretical model used to calculate the electronic structure, and the derived properties. In section 3, we present and discuss the results of our calculations and compare them with experimental data. Our conclusions are given in section 4.

2. Theoretical approach

Clusters with 19 atoms, as shown in figure 1, were chosen to represent the FCC Fe–Pd alloys. In all these clusters, the Fe or Pd atom of special interest is located at the centre, which is surrounded by 12 nearest neighbours (NNs) and six next-nearest neighbours (NNNs). Since the central atom in a cluster has complete NN and NNN shells, its environment in the cluster is closest to that of an infinite crystal and is that showing the most bulk-like properties, as has been confirmed by many calculations on metallic clusters [15–17]. Therefore we have chosen in all cases the central site, occupied by an Fe atom or Pd atom, for the evaluation of local properties.

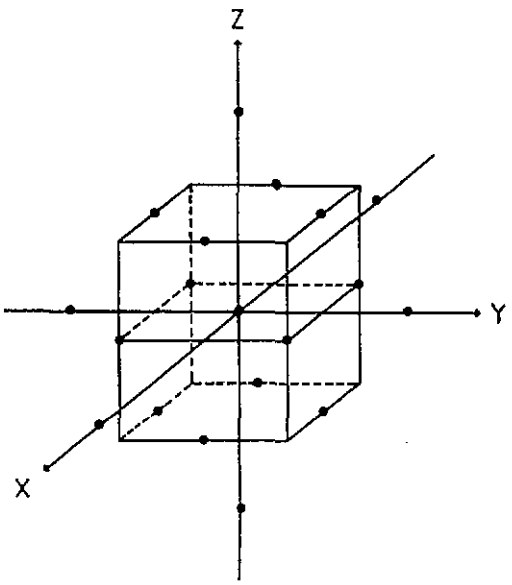

Figure 1. The geometry of the 19-atom cluster used to model the FCC Fe–Pd alloys.

The electronic structure of the clusters was obtained using a linear combination of atomic orbitals (LCAO) DVM, within the framework of the density-functional theory and the local-spin-density approximation. Self-consistent one-electron wavefunctions were derived by solving the Hartree–Fock–Slater equation

$$(h_\sigma - \epsilon_{i\sigma})\Phi_{i\sigma} = [-\tfrac{1}{2}\nabla^2 + V_{\mathrm{Coul}}(\rho_\sigma) + V_{\mathrm{xc}}(\rho_\sigma) - \epsilon_{i\sigma}]\Phi_{i\sigma} = 0.$$

The Coulomb potential $V_{\mathrm{Coul}}(\rho_\sigma)$ includes both electron–electron and electron–nucleus interactions. The spin-dependent exchange–correlation potential $V_{\mathrm{xc}}(\rho_\sigma)$ was chosen to be of the spin-polarized von Barth–Hedin [18] form. The electronic density $\rho_\sigma(r)$ for each spin σ is given by

$$\rho_\sigma(r) = \sum_i n_{i\sigma}|\Phi_{i\sigma}(r)|^2$$

where $n_{i\sigma}$ is the occupation of the cluster spin orbital $\Phi_{i\sigma}(r)$, determined by Fermi–Dirac statistics. The molecular spin orbitals $\Phi_{i\sigma}$ are expanded as a linear combination of numerical symmetrized atomic orbitals:

$$\Phi_{i\sigma}(r) = \sum_j \chi_j^s(r)C_{ji}^\sigma.$$

Then the secular equations $(\mathbf{H} - E\mathbf{S})\mathbf{C} = \mathbf{0}$ are derived, where $\mathbf{H}$ is the energy matrix, $\mathbf{S}$ the overlap matrix and $\mathbf{C}$ the matrix of the eigenvectors. All matrix elements are calculated numerically on a random-point grid by the diophantine method [19]. The eigenvectors and eigenvalues are derived by solving iteratively the secular equations.

The atomic basis set of the form $R_{nl}Y_{lm}(\theta, \varphi)$, where $R_{nl}(r)$ are numerical radial functions, gives the solutions of the self-consistent-field Schrödinger equation for Fe and Pd atoms in their spherical potential wells. In the variational expansion of the cluster spin orbitals $\Phi_{i\sigma}(r)$, the numerical atomic orbitals 3s, 3p, 3d, 4s and 4p for central Fe are included. For other Fe atoms, only the 3d, 4s and 4p are kept in the variational basis; for Pd, 4d, 5s and 5p are included. The remaining low-lying orbitals are used to build the potential but are frozen after the first cycle in all cases. The valence orbitals are orthogonalized with respect to the core.

The actual electronic density is fitted to a model variational charge density $\rho_\sigma^{\mathrm{scc}}(r)$ (the superscript scc indicates self-consistent charge), which is a superposition of radial densities R_{nl}^ν centred on cluster atoms via the diagonal-weighted Mulliken population f_{nl}^ν:

$$\rho_\sigma^{\mathrm{scc}}(r) = \sum_{nl}\sum_\nu f_{nl}^\nu |R_{nl}(r_\nu)|^2.$$

The coefficients f_{nl}^ν are determined variationally in each cycle by a least-squares error minimization procedure, with the condition that $\rho_\sigma^{\mathrm{scc}}(r)$ integrates to the total number of electrons in the cluster. Self-consistency is achieved through convergence of these coefficients, which is the so-called self-consistent charge approximation.

In order to represent better the solid by a cluster, an embedding scheme [19] is employed to simulate the effect of the rest of the microcrystal on the cluster, i.e. all clusters are embedded in an Fe–Pd microcrystal which is the periodic translation of the corresponding cluster; it consists basically of placing numerical atomic potentials at about 300 sites surrounding the cluster. The embedding potentials are derived from a superposition of electronic densities of atoms placed at the crystal sites exterior to the cluster. These

potentials are truncated by means of pseudopotentials in order to simulate orthogonality effects. For a reliable comparison, all input parameters, such as the atomic basis functions, integration points and crystal potentials were kept fixed.

For FCC disordered Fe–Pd alloys, the lattice constants change less than 3% in the whole concentration range [20]. In our calculations, the variation in lattice parameters with concentration is neglected and no local distortion is assumed. All results have been obtained for the FCC Pd lattice parameter of 3.88 Å. Thus the electronic effects of various local atomic compositions are thought to contribute to the variations in local environments of the central atom. For convenience, Fe-centred and Pd-centred clusters are denoted by *Fe(P, Q) and Pd(P, Q), respectively, where P and Q are the numbers of Fe atoms in the* NN and NNN shells, respectively. There are various locations for NN Fe atoms, which we have considered to represent several possible local environments with high symmetry, as follows: 12Fe NN + 6Fe NNN and 12Pd NN + 6Fe NNN in O_h symmetry, (10Fe + 2Pd) NN + 6Fe NNN and (2Fe + 10Pd) NN + 6Fe NNN in D_{2h} symmetry, (8Fe + 4Pd) NN + 6Fe NNN and (4Fe + 8Pd) NN + 6Fe NNN in D_{2d} symmetry, and (6Fe + 6Pd) NN + 6Fe NNN in D_{3d} symmetry.

3. Results of calculations and discussion

3.1. Results for the Fe site

3.1.1. Magnetic moment and charge transfer. Table 1 shows the local magnetic moments and electron occupation numbers of the central Fe atom, which are determined from a Mulliken population analysis. The results for the NN Pd atom are also listed in table 1 so that the relation between the central Fe atom and its local environment can be better understood.

Table 1. Local magnetic moments μ_i and occupation numbers n_i for the Fe-centred clusters. Fe(N, M) indicates the cluster with N and M Fe atoms at the NN and NNN shells.

		Central Fe							NN Pd	
Cluster	Symmetry	μ_{3d} (μ_B)	μ_{4s} (μ_B)	μ_{4p} (μ_B)	μ_{Fe} (μ_B)	n_{3d}	n_{4s}	n_{4p}	μ_{4d} (μ_B)	μ_{5s+5p} (μ_B)
Fe(12, 6)	O_h	3.10	−0.04	−0.16	2.90	6.34	0.78	0.60		
Fe(10, 6)	D_{2h}	3.20	−0.02	−0.09	3.09	6.35	0.79	0.61	0.13	−0.26
Fe(8, 6)	D_{2d}	3.24	0.00	−0.08	3.16	6.32	0.76	0.55	0.23	−0.18
Fe(6, 6)	D_{3d}	3.33	0.01	−0.01	3.33	6.32	0.75	0.47	0.29	−0.06
Fe(4, 6)	D_{2d}	3.32	0.05	0.01	3.38	6.26	0.72	0.46	0.28	−0.08
Fe(2, 6)	D_{2h}	3.38	0.07	0.03	3.48	6.27	0.69	0.40	0.27	−0.09
Fe(0, 6)	O_h	3.42	0.10	0.05	3.57	6.29	0.68	0.33	0.28	−0.04

The cluster Fe(12, 6) representing FCC γ-Fe with a lattice constant of 3.88 Å was calculated first. From table 1, the total magnetic moment in such an assumed FCC phase is found to be $2.9\mu_B$ per Fe atom. In recent years, several attempts have been made to establish the magnetic properties of the FCC phase of iron from both experimental investigations [21–23] and theoretical calculations [24, 25]. Different workers have reported contradictory experimental results. Theorists found that the ground state depends sensitively on the volume so that magnetic phase transitions may occur when the experimental conditions are changed.

Our results show that the FCC phase of iron with a lattice parameter of 3.88 Å is in the high-spin ferromagnetic state, which is consistent with the band-structure calculations. It needs to be noted that there is a finite cluster effect because the overlap of orbital wavefunctions in the cluster is not so complete as in the bulk solid, and the calculated magnetic moment using the molecular cluster method is somewhat larger than the value of the band-structure method [15, 16], but the cluster model tends to the same limit as the band-structure results as the cluster size is increased. In treating the alloy properties, where local order may be a dominant factor rather than long-range periodicity, representation of the system by small embedded clusters is not only computationally attractive but also physically reasonable. For most physical properties, it has been justified that the three- to four-atom-shell cluster is sufficient [15] and, for the magnetic moment of the alloys, one can focus on trends instead of absolute values.

In table 1, it may be seen that Fe atoms have large positive magnetic moments for our calculated cases. These results show that FCC Fe–Pd alloys are strong ferromagnets, and the Fe atoms of these alloys are in the high-spin state. From the behaviour of the magnetic moments as a function of the number of Pd NNs it is found that μ_{Fe} shows a slight increase with the addition of Pd atoms in the first shell of neighbours, while the 3d local moment μ_{3d} is almost independent of the number of Pd neighbours. Such a tendency is in satisfactory agreement with the results of the neutron-scattering data [8]. The 4s and 4p conduction band moments μ_{4s} and μ_{4p} change gradually from negative to positive for more than about six NNs of Pd atoms.

Now let us turn to the results of NN Pd atoms. Although their values are less accurate, and the detailed analysis of the Pd properties in the clusters, where the Pd atom is at the central site, will be given in section 3.2, the general features of Pd atoms in the Fe–Pd alloys are exhibited in table 1. It is clear that Pd atoms, with a large positive induced magnetic moment, are strongly polarized; this has not been found in other transition-metal alloys with iron, such as Fe–Cu and Fe–Ag [26].

Charging effects are important to the formation of alloys. Table 1 also shows the numbers of d, s and p electrons at the central Fe site, as determined by the Mulliken population analysis. Both the s- and p-electron counts decrease with the increase in Pd atoms in the NN shell. Charge transfer from Fe valence orbitals to Pd neighbours takes place, which is consistent with the difference between their electronegativities: Fe, 1.8; Pd, 2.1. Watson and Bennett [27] used a renormalized atom model to suggest that the charge flow in the transition-metal alloys and compounds is such that the d-electron flow is in the opposite direction to the non-d-electron flow. The present results seem to deviate from the above rule; the number of 3d electrons changes very little when there are no more than six Pd atoms as NNs; then a sudden decrease occurs when the central Fe atom is surrounded by eight Pd and four Fe atoms in the NN shell. Finally the number of 3d electrons increases, as predicted by Watson and Bennett, when more and more Pd atoms are in the first-neighbour shell. We believe that this unusual result does not represent an intrinsic property of the Fe–Pd alloys but may result from neglecting the lattice parameter change with concentrations and the magnetovolume effect.

3.1.2. Hyperfine fields. The hyperfine field is a short-range parameter, which mainly depends on the local environment of the probe nucleus. The Fermi contact contribution to the hyperfine magnetic field is defined [28] as

$$H_{hf} = \tfrac{8}{3}\pi g\mu_B(\langle S\rangle/P)[\rho_\uparrow(0) - \rho_\downarrow(0)] = B\Delta\rho(0)$$

where S is the total spin of the Fe with P unpaired electrons, the term $\rho_\uparrow(0)-\rho_\downarrow(0) = \Delta\rho(0)$ is the electronic spin density at the Fe nucleus, and $B = 524.2(e/a_0^3)^{-1}$ kG is the proportionality constant.

The 3s and valence band contributions to H_{hf} are obtained in our calculations directly from the self-consistent molecular orbitals. Considering numerical accuracy and basis-set incompleteness, the core contributions are better obtained from atomic local-spin-density calculations for the same configuration that Fe has in the cluster and the same exchange–correlation potential (von Barth–Hedin).

We have calculated the hyperfine fields for six distinct local configurations representing the FCC disordered Fe–Pd alloys using the above equation, which are listed in table 2. For comparison we calculate the 15-atom cluster $FeFe_8Fe_6$, representing α-Fe. The calculated H_{hf} of -429 kG is significantly larger than the experimental value of -339 kG for α-Fe. It should be pointed out that, apart from the cluster-size effects, the form of the local exchange interaction used and relativistic effects can strongly affect the hyperfine field in a local-density calculation.

Table 2. Hyperfine fields H_{hf} for Fe–Pd clusters. N is the number of NN Fe atoms.

Cluster	Symmetry	H_{hf} (kG)	ΔH_{hf} (kG)	$\Delta H_{hf}/N$ (kG)	Experimental $\Delta H_{hf}/N$ [a] (kG)
$FeFe_8Fe_6$	O_h	−429			
Fe(10, 16)	D_{2h}	−416	13	6.5	
Fe(8, 6)	D_{2d}	−401	28	7.0	9
Fe(6, 6)	D_{3d}	−380	49	8.2	
Fe(4, 6)	D_{2d}	−353	76	9.5	
Fe(2, 6)	D_{2h}	−350	79	7.9	
Fe(0, 6)	O_h	−334	95	7.9	

[a] From [9].

The magnetic hyperfine field H_{hf} at the Fe site is often regarded as a measure of the magnetic moment on the Fe atom. However, this relation is questionable to some extent [29,30] if one considers the terms contributing to H_{hf}. In table 2, the hyperfine fields decrease with the addition of Pd atoms in the NN shell, although the magnetic moment of the central Fe atom slightly increases. We would like to point out that, where the moment of the 4s electrons is positive, the ferromagnetic alignment of the Fe 4s with respect to the Fe 3d moment gives rise to an excess of majority-spin 4s electrons at the Fe nucleus; so their contribution to H_{hf} is also positive, lowering the total (negative) hyperfine field. A change in the sign of the polarization of the 4s conduction electrons relative to bulk Fe led to opposite variation in the magnetic moment versus the magnetic hyperfine field.

Although all calculated values are somewhat too large in comparison with the experimental hyperfine fields, from the tendency with the number of Pd atoms in the NN shell, the calculated H_{hf} is consistent with the experimental data. Furthermore, we have calculated the difference between these clusters using

$$\Delta H_{hf} = H_{hf}(\text{alloy}) - H_{hf}(\alpha\text{-Fe})$$

and also listed the results in table 2. It can be seen that the hyperfine field is reduced by about 8 kG for each Fe atom which is replaced by a Pd atom in the first-neighbour shell. Our result is in good agreement with the experimental value obtained from analysing Mössbauer spectra [9], which is about 9 kG at 4.2 K. It is worth pointing out that the effects

mentioned above which influence the absolute value of H_{hf} are partially cancelled when we calculate ΔH_{hf}. This may be partially responsible for the observed good agreement between our result and experiment.

3.1.3. Density of states. Now let us consider the density of states (DOS), which is a very important quantity for understanding the energy spectrum of the valence eigenfunctions. For the cluster model, the total DOS does not compare very well with band-structure calculations owing to the finiteness of the cluster [15]; here we consider only the local DOS corresponding to a volume surrounding the central atom, which is rather independent of cluster size and shows the most bulk-like properties.

The local DOS is defined as

$$D^{\nu}_{nl}(E) = \sum_{p} f^{\nu}_{nl,p} \frac{\sigma/\pi}{(E-\epsilon_p)^2+\sigma^2}$$

where $f^{\nu}_{nl,p}$ is the Mulliken population contribution from atom ν, state (n,l) to the pth molecular orbital corresponding to the energy ϵ_p. The Lorentzian width parameter σ was chosen to be 0.1 eV.

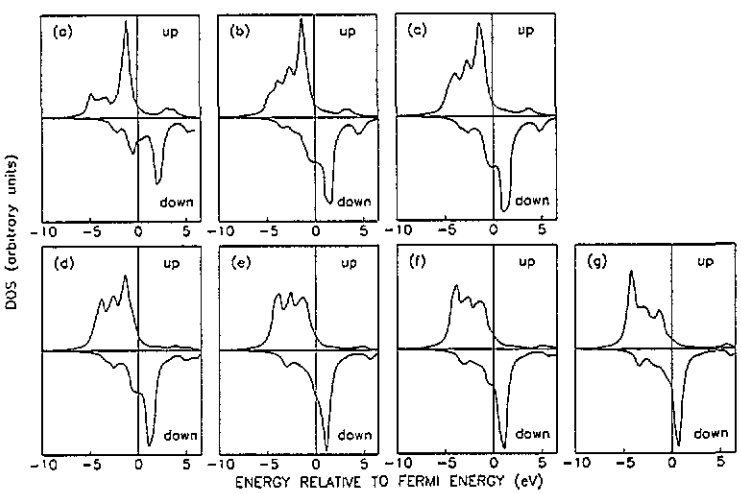

Figure 2. Local DOSs for the central Fe 3d majority spin (up) and minority spin (down): (*a*) 15-Fe-atom cluster; (*b*) Fe(10, 6); (*c*) Fe(8, 6); (*d*) Fe(6, 6); (*e*) Fe(4, 6); (*f*) Fe(2, 6); (*g*) Fe(0, 6). The majority-spin and minority-spin bands are normalized to the same scale within each cluster.

Figure 2(*a*) shows the central Fe 3d DOS of the 15-atom cluster representing α-Fe for comparison, which is taken from our previous calculation [26]. Figures 2(*b*)–2(*g*) depict the local 3d DOSs for the central Fe atom in six distinct cluster environments. From these figures, a general trend can be observed as the number of Pd NNs increases.

(1) The minority-spin 3d states show multipeak structures of reduced magnitude below the Fermi level and an increased sharp peak above the Fermi energy. The positions of these peaks hardly change relative to the Fermi level. Thus the 3d moment is almost unaffected by the number of Pd NNs.

(2) For the majority-spin 3d states, the small peak at low energy becomes larger while the main peak near the Fermi level becomes smaller, and a broad multipeak structure

extends almost to the energies corresponding to the Pd d band [31]. With the increase in number of Pd atoms in the NN shell, the weight of the majority-spin 3d states moves to the lower-energy position, which shows that strong Fe d and Pd d hybridization occurs. The interaction between Fe and Pd results in a very small number of majority-spin states near the Fermi level and, in a sense, the Fe–Pd alloys become strong ferromagnets.

It is worth pointing out that hybridization effects are very important for Fe–Pd clusters. Unlike the Cu–Fe and Ag–Fe clusters [26], where the interactions of the 3d electrons of Fe are predominantly with the s and p electrons of Cu and Ag owing to the deep-lying filled d shell for Cu and Ag, the hybridization in Fe–Pd alloys is mostly between Fe 3d and Pd 4d and causes a large polarization of the Pd atoms in the positive direction.

3.2. *Results for the Pd site*

Above we have studied the behaviour of the local magnetic moment and the contact hyperfine field of a central Fe site in Fe–Pd clusters versus changes in the number of Pd atoms in the first coordination shell. In order to understand completely the properties of Fe–Pd alloys, the results for a central Pd atom in 19-atom clusters are presented below.

3.2.1. Magnetic moment. Table 3 lists the Pd magnetic moments. As mentioned above, the Pd atoms in Fe–Pd alloys are shown to be strongly polarized. From table 3, it may be seen from our calculations that there is a large positive 4d magnetic moment of Pd, while the 5s + 5p moment is small and negative, so that the total magnetic moment still has a positive value.

Table 3. Calculated Pd atom magnetic moment. Pd(N, M) indicates a Pd-centred cluster with N and M Fe atoms at NN and NNN shells.

Cluster	Symmetry	μ_{4d} (μ_B)	μ_{5s+5p} (μ_B)	μ_{Pd} (μ_B)
Pd(2, 6)	D_{2h}	0.26	−0.01	0.25
Pd(4, 6)	D_{2d}	0.28	−0.03	0.25
Pd(6, 6)	D_{3d}	0.42	−0.06	0.36
Pd(8, 6)	D_{2d}	0.39	−0.13	0.26
Pd(10, 6)	D_{2h}	0.36	−0.19	0.17

By analysing table 3, it is found that the Pd 4d moment increases with the number of NN Fe atoms, until it reaches its largest value when the central Pd is surrounded by six Fe and six Pd atoms. With more Fe atoms in the first coordination shell, the Pd 4d moment (and consequently its total magnetic moment) decreases. By using neutron-scattering and magnetization measurements, Cable *et al* investigated a series of FCC Fe–Pd alloys, determined the distribution of magnetic moments and found that the average Pd moment increases with increasing Pd concentration and reaches a maximum of about $0.4\mu_B$ in the concentrated alloys [8]. Our results are in fairly good agreement with the experimental data of Cable *et al*.

3.2.2. Density of states. Figure 3 depicts the central Pd 4d DOSs for several clusters with distinct local environments.

For these diagrams, an apparent difference between the two spin directions is that the majority and minority DOSs differ with increasing Fe content, and polarization effects exist for the Pd DOS in the Fe–Pd alloys.

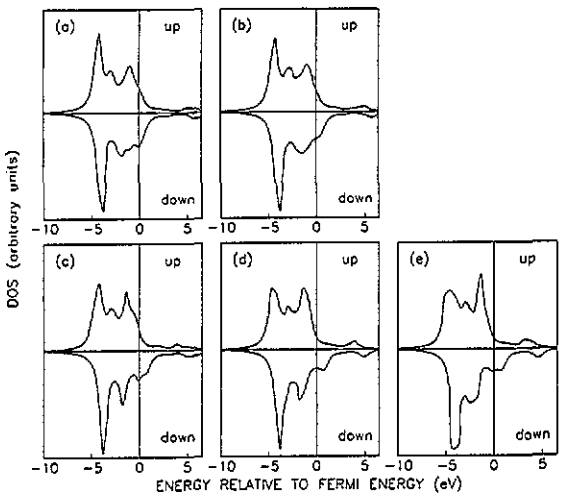

Figure 3. Local DOSs for the central Pd 4d majority spin (up) and minority spin (down): (*a*) Pd(2, 6); (*b*) Pd(4, 6); (*c*) Pd(6, 6); (*d*) Pd(8, 6); (*e*) Pd(10, 6).

Furthermore, it is found that, on increase in the number of NN Fe atoms, large changes in the majority-spin 4d states take place, including a variation in the multipeak structures, a downward displacement of the position of the whole majority-spin 4d DOS and a decrease in the DOS at the Fermi level for majority-spin states. In contrast with the majority-spin 4d states, the minority-spin 4d states change little.

All these features of the central Pd 4d DOSs result from hybridization of the Fe 3d and Pd 4d states. According to the band-structure calculation [31], the 4d bands of Pd extend slightly above the Fermi level, and Pd has the fewest d-band holes of the transition-metal d bands. The majority-spin 3d states of Fe are distributed over the lower part of the 4d bands which mainly hybridizes with the majority-spin 3d states of Fe. Such an interaction results in a positive polarization of Pd 4d electrons.

4. Conclusions

The spin-polarized DVM in the local-density approximation has been employed to obtain the electronic structures of a central Fe site and central Pd site in a number of embedded clusters representing FCC Fe–Pd alloys. Several possible environments of atoms around Fe and Pd sites in the alloy have been considered in order to study the properties such as magnetic moments, hyperfine fields and the DOS. Our calculated results show the following.

(1) The Fe 3d magnetic moment is almost independent of the number of Pd NNs; its total moment slightly increases with increasing number of Pd NNs.

(2) Pd atoms are strongly polarized and a large induced magnetic moment exists for Pd atoms in Fe–Pd alloys, which results from the large hybridization of the Fe 3d and Pd 4d states. When the Pd atom is surrounded by six Fe and six Pd NNs, it has its maximum induced moment, which compares quite well with neutron-scattering data.

(3) The hyperfine fields at the Fe nucleus slightly decrease with increasing number of NN Pd atoms. The variation in hyperfine fields is consistent with Mössbauer data.

From our studies, we concluded that the cluster model is a very efficient technique for investigating the local properties, especially in treating disordered transition alloys.

Acknowledgment

This work was performed on a DEC-5000 at the Institute of Physics, Academia Sinica.

References

[1] Nakamura M, Sumiyama K and Shiga M 1979 *J. Magn. Magn. Mater.* **12** 127
[2] Shiga M, Muraoka Y and Nakamura Y 1979 *J. Magn. Magn. Mater.* **10** 280
[3] Matsui M, Shimizu T, Yamada H and Adachi K 1980 *J. Magn. Magn. Mater.* **15–18** 1201
[4] Nakayama T, Kikuchi M and Fukamichi K 1980 *J. Phys. F: Met. Phys.* **10** 715
[5] Gerstenberg D 1958 *Ann. Phys., Lpz.* **2** 236
[6] Crangle J 1960 *Phil. Mag.* **5** 335
[7] Bozorth R, Wolff P A, Davis D D, Compton V B and Wernick J H 1961 *Phys. Rev.* **122** 1157
[8] Cable J W, Wollan E O and Koehler W C 1965 *Phys. Rev.* **138** A755
[9] Zhang S L, Sumiyama K and Nakamura Y 1988 *J. Magn. Magn. Mater.* **73** 58
[10] Wolff P A 1961 *Phys. Rev.* **124** 1030
[11] Clogston A M, Matthias B T, Peter M, Williams H J, Corenzwit E and Sherwood R J 1962 *Phys. Rev.* **125** 541
[12] Moriya T 1965 *Prog. Theor. Phys.* **34** 329
[13] Delley B, Ellis D E and Freeman A J 1982 *J. Magn. Magn. Mater.* **30** 71
[14] van Acker J F, Speier W and Zeller R 1991 *Phys. Rev.* B **43** 9558
[15] Guenzburger D and Ellis D E 1985 *Phys. Rev.* B **31** 93
[16] Chacham H, Galvão da Silva E, Guenzburger D and Ellis D E 1987 *Phys. Rev.* B **35** 1602
[17] Press M R, Khanna S N and Jena P 1987 *Phys. Rev.* B **36** 5446
[18] von Barth U and Hedin L 1972 *J. Phys. C: Solid State Phys.* **5** 1629
[19] Ellis D E 1968 *Int. J. Quant. Chem. Symp.* **2** 35
Ellis D E and Painter G P 1970 *Phys. Rev.* B **2** 2887
[20] Pearson W B 1958 *A Handbook of Lattice Spacings and Structures of Metals and Alloys* (Oxford: Pergamon) p 633
[21] Montano P A, Fernando G W, Cooper B R, Moog E R, Naik H M, Bader S A, Lee Y C, Darici Y M, Min H and Marcano J 1987 *Phys. Rev. Lett.* **59** 1041
[22] Prescia D, Stampanoni M, Bona G L, Vaterlaus A, Willis R F and Meier F 1987 *Phys. Rev. Lett.* **58** 2126
[23] Macedo W A A and Keune W 1988 *Phys. Rev. Lett.* **61** 475
[24] Moruzzi V L, Marcus P M, Schwarz K and Mohn P 1986 *Phys. Rev.* B **34** 1784
[25] Moruzzi V L, Marcus P M and Kübler J 1989 *Phys. Rev.* B **39** 6957
[26] Cai J W, Luo H L, Zeng Z and Zheng Q Q 1992 *J. Phys.: Condens. Matter* **4** 8813
[27] Watson R E and Bennett L H 1978 *Phys. Rev.* B **18** 6439
[28] Watson R E and Freeman A J 1961 *Phys. Rev.* **123** 2027
[29] Callaway J and Wang C S 1977 *Phys. Rev.* B **16** 2095
[30] Duff K J and Das T P 1971 *Phys. Rev.* B **3** 2294
[31] Moruzzi V L, Janak J F and Williams A R 1978 *Calculated Electronic Properties of Metals* (Oxford: Pergamon) p 144